Preventing battery thermal runaway via electro-thermal characterization using impedance spectrum

Pragya Berwal and Jack J. Yoh
Aerospace Engineering Department, Seoul National University
Seoul, South Korea

1 Introduction

A shift towards clean and green energy sources has rapidly increased the demand for electric vehicles (EVs) utilizing lithium-ion batteries (LIBs). In general, LIBs kinetics and safety experimental studies are conducted for their thermal and electrical characterization. Thermal characterization is studied using calorimetry to acknowledge rate of heat change with respect to temperature or time via thermal degradation [1]. Alternatively, thermal runaway (TR) in LIBs is also observed due to internal resistive heating/joule heating leading to internal short circuits and fire accidents. In particular, direct current (DC) pulses over time domain and alternating current (AC) signal over frequency domain are passed through sample battery cell for electro-thermal characterization and determining battery safety based on joule heating [2]. The present work utilizes AC signals over frequency domain to investigate the electrical parameters utilizing the electrochemical impedance spectroscopy (EIS). EIS technique is based on the perturbation of an electrochemical system in equilibrium via applying a sinusoidal AC signal over a range of frequencies. EIS is utilized on a linear time-invariant system, and the response of the input signals is obtained in the form a transfer function, namely impedance. The technique is preferred over voltametric techniques utilizing DC pulses due to its comprehensive characterization of internal processes, non-destructive nature with real-time monitoring of battery health, and quantitative evaluation of battery resistance [3].

Ender et al. [4] reported EIS research on lithium iron phosphate (LFP) cathode with lithium metal as anode to establish the electrode misalignment impact on impedance signals. They reported the presence of cross contamination in impedance response due to inductive reactance and therefore suggested that symmetry between two electrodes is necessary for better quantitative analysis. Klink et al. [5] also observed similar results for LFP battery cell and reported an error of 5% in impedance values due to asymmetric geometry between the electrodes. Ovejas et al. [6] utilized EIS measurement technique to characterize the transport and chemical phenomena occurring in LIB consisting of $LiCoO_2$-$Li[NiMnCo]O_2$ (LCO-NMC) as cathode and graphite as anode. The studies reported that LCO-NMC electrode charge transfer is more affected by ageing of the battery in comparison to solid electrolyte interface (SEI) layer. 70% reduction in electrochemical process was also observed due to decrease in characteristic frequency of the battery system with the ageing effect.

Choi et al. [7] explained the impedance spectrum depicted via Nyquist plots. The resistance due to current collectors, electrolyte, and separator is collectively termed as ohmic resistance and is depicted

Correspondence to: jjyoh@snu.ac.kr

by the x-axis intercept value of Nyquist plot. The first semi-circular part defines the formation of SEI layer deposited on the electrode and second semi-circle represents the faradaic charge-transfer resistance related to kinetics of electrochemical reaction taking place inside the battery. Lastly, the straight line of the plot is related to the diffusion of the lithium ions. Although a general understanding of the Nyquist plot was established for a battery system, the detailed description based on state of charge (SOC), ageing, and temperature conditions are yet to be studied. With the intention of expanding our horizon of EIS data using Nyquist plot, the present study utilizes LFP as cathode and silicon carbon nanocomposite (SCN) as anode to investigate the impedance spectrum with the changes in SOC from 0% to 100%. The variations of exchange current density and time constant with SOC are also discussed to acknowledge the effect of SOC on battery safety.

2 Methodology

2.1 Electrical Characterization

The present study utilizes ZiveLab SP2 workstation embedded with frequency response analyzer (FRA) for impedance measurement. An electrochemical interface applies constant voltage which is superimposed with sinusoidal AC signal to obtain EIS results. A multiplexer connects the FRA with the battery system. The battery coin cell prepared in-house is shown in Fig. 1(a). For coin cell preparation, the cathode and anode layers of 16 mm diameter and separator of 20 mm diameter is cut using a punching machine. Separator of larger diameter is cut to ensure proper separation of cathode and anode in order to avoid internal short circuit. Separator material of polyethylene/polypropylene is dipped in electrolyte (EC/DMC/DME) as utilized by the commercial industry. The coin cell is prepared inside argon glove box to avoid sample contamination. The layered coin cell is sealed with a spacer and wave spring inside using a cell crimper. Spacer and wave spring is utilized to ensure consistent contact between electrodes and separator with uniform force. The prepared LFP/SCN coin cell is connected to EIS workstation SP2 using 4 connecting wires: two each for current flow and cell potential. The frequence range of 0.1 Hz to 100 kHz is applied to measure the response of input signal. The present study utilizes EIS under potentiostatic mode i.e. constant voltage, where voltage is applied at each frequency and current is measured as response. To ensure steady state condition, a small voltage amplitude of 10 mV is applied to obtain pseudo-linear cell response. The impedance, Z, obtained via EIS response is a frequency dependent complex transfer function defined using Ohm's law as follows:

$$Z = \frac{V_o \sin(\omega t)}{I_o \sin(\omega t + \phi)} = |Z| e^{i\Phi} = Z' + iZ'' \ \ where\ i = \sqrt{-1} \quad (1)$$

Here, V_o and I_o are peak voltage and current of the AC signal, ω is the frequency (in Hertz, Hz) and ϕ is the phase shift between AC voltage and current signal. The Nyquist plot studied under section 3 represents the relation between real (Z') and imaginary (Z'') part of the impedance on a linear scale. The ohmic (R_e) and polarization resistance (R_{ct} & Z_w) gives rise to LIB heating known as joule heating (Q_{joule} or $Q_{\text{electrical}}$) equated as:

$$\dot{Q}_{\text{joule}} = I^2(R_e + R_{ct} + Z_w) \text{ Watts} \quad (2)$$

2.2 Chemical Characterization

The combustion theory for LIB is developed in our previous work [8] using the real-time enthalpy data with respect to temperature, measured using DSC (Differential Scanning Calorimetry) for battery system under varying SOCs (0% ~ 100%). Realistic values of convective heat transfer coefficient (h) for both natural and forced convection cooling strategies are employed to contemplate the heat losses and define the thermal characteristics of LIB due to chemical reaction. The chemical heat generation ($Q_{chemcial}$) in Watts considers the Arrhenius law for thermochemical reactions taking place inside a LIB that deals with solid electrolyte interface, cathode decomposition, and chemical reaction between cathode and anode.

$$\dot{Q}_{\text{chemical}} = m_o \Delta H A \exp\left(\frac{-E}{R\,T}\right) \quad (3)$$

$$\dot{Q}_{\text{cooling}} = h\,A_S(T - T_0) \quad (4)$$

Here, m_o is the sample mass of the cell under study, ΔH is heat of reaction (J/kg), A is pre-exponential factor (s^{-1}), E is the activation energy (J/mol), T is the sample temperature (K) and R is the universal gas constant (J/mole-K). A_S is the surface area of heat transfer (m^2) and T_0 is the ambient temperature i.e. 298 K of the sample before testing. The energy equation considering total heat generation and heat loss is given as follows:

$$\dot{Q}_{\text{total}} - \dot{Q}_{\text{cooling}} = m_o c_P \frac{dT}{dt} \quad \text{where; } \dot{Q}_{\text{total}} = \dot{Q}_{\text{joule}} + \dot{Q}_{\text{chemical}} \quad (5)$$

Figure 1(b) represents the variation of total heat generation and cooling curves with respect to temperature to determine the TR characteristics. Equilibrium temperature (T_E) is determined where the heat generated by LIB equals the cooling curve, whereas the inflection temperature (T_M) refers to the maximum temperature until which acceleration in heat generation of the system is observed. $T_{E2} > T_M$ suggests a safety operation zone to avoid TR whereas $T_{E1} < T_M$ leads to an absolute TR occurrence, namely a point of no-return for two different cooling curves.

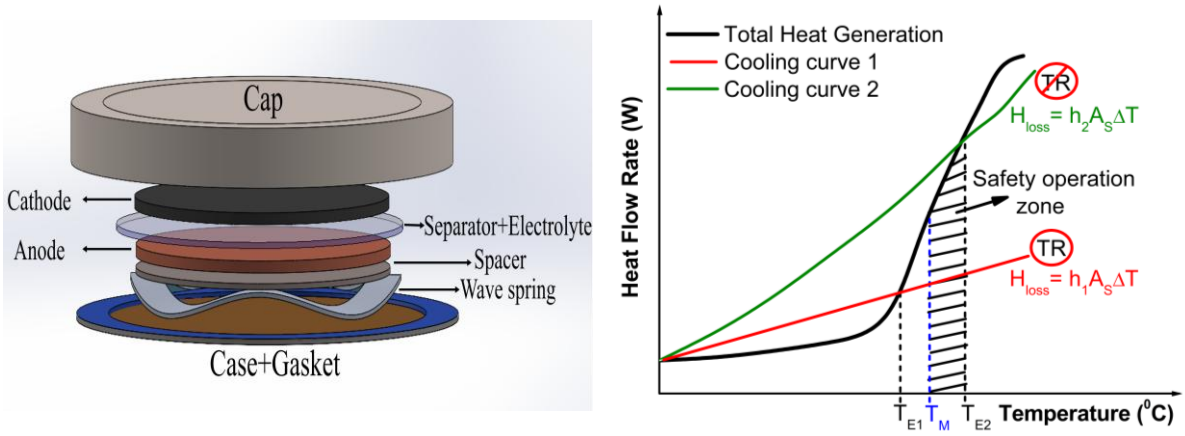

(a) (b)

Figure 1: (a) 3-D model of prepared LFP/SCN coin cell (b) Heat Flow rate of LIB sample versus temperature depicting developed combustion theory

3 Results & Discussion

Figure 2(a) shows the Nyquist plot of LFP-LIB coin cell utilizing EIS under varying SOC (0% - 100%). The Nyquist plot displayed impedance data for a range of frequencies (0.1 Hz – 100 kHz) which helps in understanding the electrochemical reactions occurring in a LIB at various potentials. EIS provides comprehensive information about the system's characteristics from fast capacitive effects to slow diffusion and reaction kinetics. This impedance data is further utilized for providing important information about cell's resistance and determines cell's power capability and joule heat. Higher the power capability, more heat is generated due to internal resistance. A semi-circle observed in Fig. 2(a) for SOC $\geq$ 50% quantifies the ohmic resistance due to electrolyte in a series connection with RC element. The RC element defines the transient electrical behavior of the battery due to polarization effects in load and charging conditions. It is observed that the semi-circular part first increases up to 75% SOC and then decreases with increase in SOC showing a non-monotonic behavior. The straight line prominently visible under lower SOCs (0% - 25%) describes the Warburg impedance which defines the dominance of ion mass diffusion over charge-transfer kinetics in an electrochemical system. Figure 2(b) depicts the

dominance of mass diffusion phenomena in heat generation at lower SOCs (tail part of Fig. 2(a)) which shift to heat generation via kinetic phenomena (semi-circular part of Fig. 2(a)) as the SOC increases.

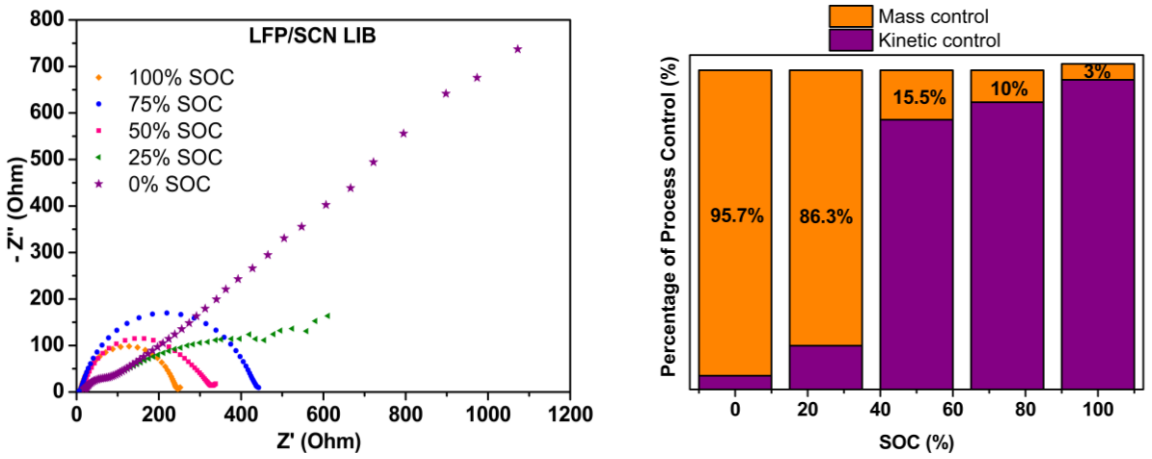

(a) (b)

Figure 2: (a) Impedance spectrum of LFP-LIB at varying SOC (b) Variation of process control percentage in heat generation with SOC

Table 1 summarizes the electrical parameters of LFP-LIB under varying SOCs for elaborating the effect of joule heating. It is observed that ohmic resistance due to electrolyte (R_e) has a small value as LFP coin cells are new and ageing effect is unprecedent to be seen. The charge-transfer resistance (R_{ct}) increases up to 75% SOC and then decreases for fully charged coin cells albeit the resistance is higher than 25% SOC. A similar trend is observed for the joule heating, which is directly proportional to a sum of ohmic and polarization resistances.

Table 1: Summary of electrical parametrization of LFP-LIB at varying SOCs

SOC (%)	Ohmic resistance, R_e (Ω)	Charge-transfer resistance, R_{ct} (Ω)	Double-layer Capacitance, C_{dl} (F)	Joule heat, Q_{Joule}	
				(kJ)	(W)
0	18.18	59.53	13.3 x 10^{-5}	0.35	1.92
25	18.4	86.1	16.0 x 10^{-5}	0.23	1.26
50	10.18	319.1	3.91 x 10^{-5}	1.23	6.79
75	6.3	435.05	5.27 x 10^{-5}	1.61	8.95
100	8.53	236.89	3.81 x 10^{-5}	0.90	4.99

Some other important parameters which define the kinetics of LIB include the exchange current density, i_0 (A/cm^2), double layer capacitance, C_{dl} and time constant, τ. The variation of such parameters with SOC is depicted in Fig. 3. A higher value of i_0 is observed at lower SOCs (0%-25%) which exacerbates diffusion limitations as increased Warburg resistance is observed (Fig. 2). This suggests that joule heat generated at lower SOCs is majorly due to poor ion diffusion coefficients, i.e. Warburg impedance. The C_{dl} represents the capacitive behavior of interface between diffused ion and electrode surface. In terms of thermodynamics, C_{dl} represents the thermal capacitance, C_{th}, of the battery system, and the heat energy stored by the LIB system is proportional to the capacitance in Farad (F) stated as follows [9]:

$$Q_{\text{stored}} = C_{\text{th}}\Delta T = \frac{1}{2}C_{\text{dl}}V^2 \qquad \Rightarrow C_{\text{th}} = C_{\text{dl}} \tag{6}$$

This defines that capacitive reactance ($X_C = 1/\omega_c C_{dl}$) increases with decrease in C_{dl} and hence joule heating increases. Figure 3 suggests a 1.7 times decrement in thermal capacitance with increase in SOC. This supports the increment of joule heat at SOC > 50% as C_{dl} reduces and Q_{stored} in a LIB system also diminishes. Time constant is a quantity which determines the quickness of a LIB system when battery

voltage stabilizes after current change. Higher values of τ at low SOCs (0%-25%) represent the slow diffusion processes which lead to higher joule heat due to Warburg impedance. With the increase in SOC > 50%, the τ reduces significantly, suggesting a fast chemical reaction kinetics and quick response. A slight increase of 5% in τ value at 75% SOC is observed due to lower exchange current density. These results again suggest that for new LFP-LIB cells, maximum joule heat is observed for 75% SOC.

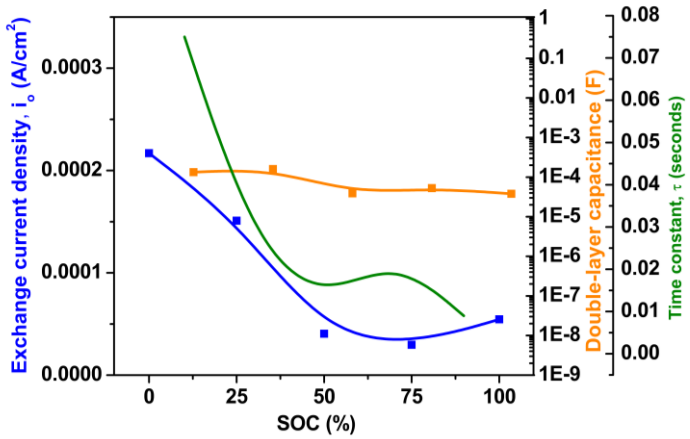

Figure 3: Variation of current density, double-layer capacitance and time constant with SOC

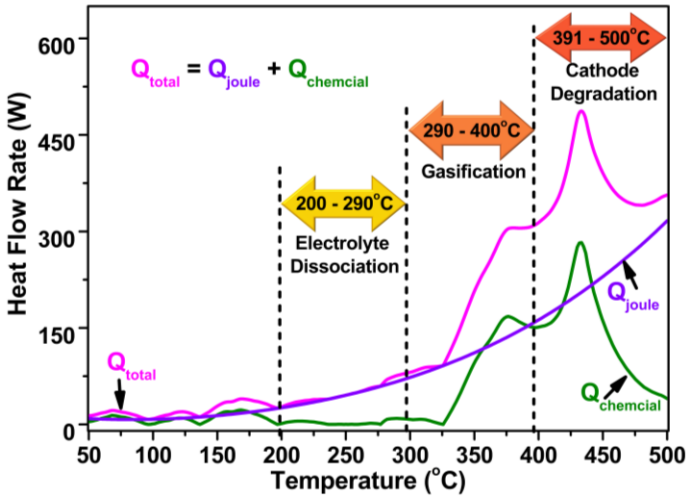

Figure 4: Variation of joule heat generation versus temperature in LFP/SCN LIB

Variation of $\dot{Q}_{total}$, $\dot{Q}_{Joule}$, and $\dot{Q}_{chemcial}$ via LFP/SCN battery cell at 100% SOC is shown in Fig. 4 for evaluating minimum convective heat transfer coefficient (h) required for preventing TR from total heat generated. $\dot{Q}_{chemcial}$ curve obtained utilizing DSC shows a heat release of 0.57 W/g and 1.13 W/g depicting gasification after SEI degradation and cathode degradation respectively. Zhang et al. [9] reported TR occurrence at ~250 ^{0}C in LFP cell utilizing DSC. They reported a peak heat flow value of 0.6 W/g at 278 ^{0}C for gasification due to SEI degradation but observed a reduced peak of 0.24 W/g at 320 ^{0}C. The discrepancy in the value of cathode degradation is observed due to variation in capacity of LFP sample used in both the studies. The present study utilizes 85 Ah LFP sample whereas Zhang et al. [9] utilizes a 280 Ah capacity LFP LIB which enhances structural stability of cathode electrode.

The combustion theory discussed in sub-section 2.2 is utilized to evaluate T_M and T_E temperatures for the total heat generation by LFP/SCN LIB system as shown in Fig. 4. Safety zone lies when $T_E \geq T_M$ as heat dissipation is higher than inflection point of heat generation [8]. It is observed that gasification and cathode degradation inflection point occurs at 362 ^{0}C and 425 ^{0}C respectively. The values of heat transfer

coefficient for various cooling curves utilizing water+glycol (50:50 by volume) mixture properties are studied in W/m^2K (Fig. 4). It is observed that to prevent TR, a minimum heat transfer coefficient of 2000 and 3320 W/m^2K is required. The total heat predicted via EIS and DSC signals help suggest a minimum warning temperature value of 243°C to prevent TR occurrence in LFP battery system of 85 Ah capacity with an effective cooling system of h = 1835 W/m^2K.

4 Conclusions

The present study deals with electro-thermal characterization of LIB leading to TR due to ohmic resistance generated via organic electrolyte during charge-transfer phenomena from working to counter electrodes. A quantitative analysis of joule heat generated through LFP-LIB cells over frequency range of 0.1Hz – 100kHz is reported under varying SOCs (0%-100%). The results suggest an increase in current density with decrease in SOC as mass transfer phenomena dominate over reaction kinetics. For 50%-100% SOC range, non-faradaic process due to formation of DLC and electrolyte produces high internal heating due to enhanced capacitive reactance values ranging from 80-132 ohms. The overall joule heating via both ohmic and polarization resistance is observed to increase by 80% with an increase in SOC as resistance increases. A battery at SOC > 50% is likely to undergo TR due to high internal resistance leading to over-heating. This impedance data can be utilized for early detection of TR observed via increased cell resistance and can further be utilized in preventing TR as a part of battery management system.

References

[1] Wulandari T., Fawcett D., Majumdar S.B. and Poinern G.E.J. (2023). Lithium-based batteries, history, current status, challenges and future perspectives. Battery Energy 2: 20230030.

[2] Lasia A. (2014). Electrochemical Impedance Spectroscopy & its Applications. Springer (ISBN : 978-1-4614-8932-0)

[3] Lazanas A.C. and Prodromidis M.I. (2023). Electrochemical impedance spectroscopy-A tutorial. ACS Meas. Sci. Au 3, 162:193.

[4] Ender M., Weber A. and Ivers-Tiffee E. (2012). Analysis of three-electrode setups for AC impedance measurements on lithium-ion cells by FEM simulations. J. Electrochem. Soc. 159(2), A128:A136.

[5] Klink S., Madej E., Ventosa E., Lindner A., Schuhmann W., and Mantia F.L. (2012). The importance of cell geometry for electrochemical impedance spectroscopy in three-electrode lithium-ion battery cells. Electrrochem. commun. 22, 120:123.

[6] Ovejas V.J. and Cuadras A. (2018). Impedance characterization of an LCO-NMC/Graphite cell: Ohmic conduction, SEI transport and Charge-transfer phenomenon. Batteries 4 : 43.

[7] Choi W., Shin H.C., Kim J.M., Choi J.Y. and Yoon W.S. (2020). Modeling and applications of electrochemical impedance spectroscopy for lithium-ion batteries. J. Electrochem. Sci. Technol. 11(1), 1:13.

[8] Berwal P., Mehrotra A., Lee Y. and Yoh J.J (2025). Combustion theory based cooling strategies for preventing thermal runaway in modern batteries. Combust. Flame. 274: 113995.

[9] Wu Y. (2015). Lithium-ion batteries: Fundamentals and Applications. CRC Press (ISBN: 978-0-4290-9688-4)

[10] Zhang Y., Cheng S., Mei W., Jiang L., Jia Z., Cheng Z., Sun J., and Wang Q. (2023). Understanding of thermal runaway mechanism of $LiFePO_4$ battery in-depth by three-level analysis. Appl. Energy. 336:120695.